

Article

Bond Performance of Seamless Steel Pipe Grouting Sleeves under Large-Deformation Repeated Tension and Compression after High Temperature

Jun Zhao ^{1,†}, Changji Wei ^{1,†}, Jing Chen ², Bin Ma ^{1,*} and Weiwei Xiao ^{1,*}

¹ School of Architecture and Transportation Engineering, Guilin University of Electronic Technology, Guilin 541004, China; zhaojun@guet.edu.cn (J.Z.); changjiwei@mails.guet.edu.cn (C.W.)

² School of Civil and Architectural Engineering, Guilin University of Technology, Guilin 541004, China; chenjing9711@gmail.com

* Correspondence: guidianmabin@guet.edu.cn (B.M.); shawwivi@guet.edu.cn (W.X.)

† These authors contributed equally to this work.

Abstract: Grouting sleeves are widely used in the field of assembled construction. The present study aims to investigate the reliability of grouting sleeves under large-deformation repeated tension and compression after high temperature, considering the influences of steel bar diameter, the cooling method, and the protective layer. Through experimentation on 28 test pieces, we analyzed the bonding performance of the test pieces at different high temperatures. The results indicate that within the temperature range of 20–800 °C, the bond performance of the test pieces declines by no more than 9.8%. However, upon reaching a temperature of 1000 °C, the bond performance of the test pieces decreases by over 33.7%, with the compressive strength of the grout material reduced to only 27.50% of that kept at 20 °C. Employing larger-diameter steel bars is advantageous for maintaining the bond performance of the test pieces. Natural cooling shows relatively good bond performance, although its influence is not significant. Furthermore, the protective layer effectively attenuates the heating rate of the test pieces, thus safeguarding their bond performance. Scanning electron microscopy (SEM) analysis reveals that the decomposition of C-H and C-S-H phases is the primary cause of high-temperature degradation of the grouting material. Finally, a recommendation for the correlation coefficient (k) between the average bond strength and the compressive strength of the grout material is proposed, with a suggested value of $k \leq 2.58$.

Keywords: grouting sleeve; high temperature; large strain of cyclic loading; prefabricated construction



Citation: Zhao, J.; Wei, C.; Chen, J.; Ma, B.; Xiao, W. Bond Performance of Seamless Steel Pipe Grouting Sleeves under Large-Deformation Repeated Tension and Compression after High Temperature. *Buildings* **2024**, *14*, 1136. <https://doi.org/10.3390/buildings14041136>

Academic Editor: Eric M. Lui

Received: 8 March 2024

Revised: 7 April 2024

Accepted: 9 April 2024

Published: 18 April 2024



Copyright: © 2024 by the authors. Licensee MDPI, Basel, Switzerland. This article is an open access article distributed under the terms and conditions of the Creative Commons Attribution (CC BY) license (<https://creativecommons.org/licenses/by/4.0/>).

1. Introduction

A grouting sleeve is a combination of connected steel bars (Figure 1) supporting grouting materials and a sleeve body, which was invented by Alfred A. Yee [1] in the 1960s and first used in the Ala Moana Hotel. Grouting sleeves are now widely used as connection parts in the field of prefabricated buildings due to their strong stability, easy installation and wide adaptability. Grouting sleeves promote the development of prefabricated buildings, and so have attracted many researchers' attention. Einea et al. [2] suggested that the anchorage length of the reinforcement could be reduced to seven times the diameter of the steel bars when the grouting materials possessed the required compressive strength. Ling et al. [3] and Hosseini et al. [4] studied the internal spiral restraint effect on the bonding stress–slip relationship of grouting sleeves. Alias et al. [5,6] studied the effects of the anchorage length of the reinforcement, the diameter of the sleeve and the internal structure of the grouting sleeve on the connection performance of grouting sleeves. Harajli et al. [7] studied the local bonding stress–slip relationship between steel bars and high-strength concrete under tensile loads. Haber et al. [8,9] studied the uniaxial tensile behavior of two kinds of commercial mechanical joints under different loading conditions, which

further confirmed the reliability of the grouting sleeve. Grouting sleeve test pieces have also been employed in research on prefabricated deep beams, joint ends, corbels, and other related areas [10,11]. In 2013, Zheng et al. [12,13] invented a new type of deformed seamless steel pipe grouting sleeve (GDPS sleeve) and carried out a series of uniaxial tensile and cyclic load tests. Their results showed that the GDPS sleeve can meet the unidirectional tensile strength requirements of class I joint specified in JGJ107-2016 [14].

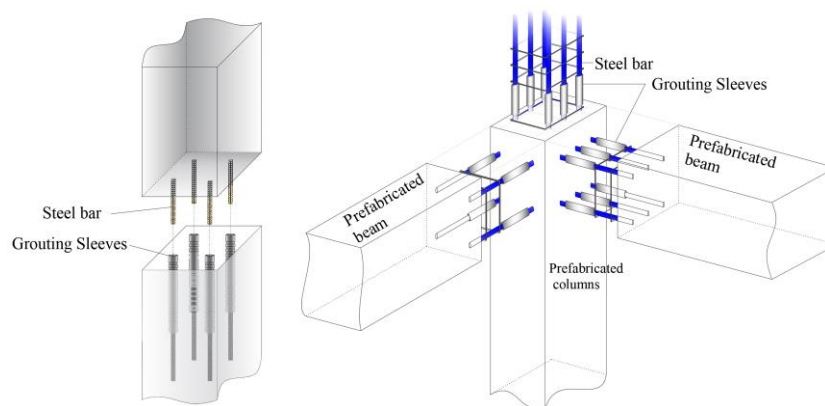


Figure 1. Application fields of grouting sleeves.

Fire directly affects the stability of prefabricated building structures. In 2022 in China, 170,000 fires were reported in self-built residential buildings, 17,000 fires were reported in high-rise buildings, and 18,000 fires were reported in various factories, resulting in a total of 1185 deaths [15]. Building fire safety is directly related to people's health and property safety, so the fire resistance of buildings has always been the research focus in the field of prefabricated buildings. Zhao et al. [16] and Xiao et al. [17] studied the connection performance of the grouting sleeve under static and dynamic loads at high temperatures and found that the temperature mainly affects the peak tensile strength of the grouting sleeve and the failure mode of the connection. Liu et al. [18,19] studied the influence of sleeve connection performance, and Zhang et al. [20,21] analyzed the bonding characteristics of grouting sleeve connections at high temperatures. They both found that the compressive strength of the grouting material decreases with the increase in temperature, and the grouting sleeve is still elastic when the temperature is below 600 °C. After the temperature exceeds 600 °C, the bonding strength of the grouting sleeve is lower than the ultimate tensile strength of the connecting steel bars. In order to study the effect of anchorage length on the tensile properties of the grouting sleeve after high temperature, Zhu et al. [22] used a semi-grouting sleeve with a diameter of 16 mm HRB400 steel bars to conduct a uniaxial tensile test at a high temperature, and found that when the temperature reached 400 °C, the optimal reinforcement anchorage length was 110 mm (7 times the steel bar's diameter). Zhu et al. [23] and Li [24] conducted tensile performance tests of grouting sleeves at high temperatures, and the results showed that a protective layer was useful for improving the ductility and tensile strength of the grouting sleeve in a high-temperature state. Chen et al. [25] and Zhang [26] conducted tensile tests on the grouting sleeve cooled with two different methods (natural cooling and water cooling) after high temperature and found that the naturally cooled grouting sleeve had better tensile performance than the water-cooled one, but the difference was not remarkable.

The seismic performance is an important index to judge the reliability of grouting sleeves, and the cyclic load test can reflect the seismic performance. Lin et al. [27] tested grouting sleeves with uniaxial tensile loading, repeated tensile loading, high-stress cyclic loading and large-strain cyclic loading. Yan et al. [28] studied the seismic performance of concrete frame beam-column connections and found that the seismic performance of the grouting sleeve connections was similar to that of the cast-in-place connections. Li et al. [29] suggested that grouting sleeves containing threads and wedges could improve the anchor-

ing performance of the sleeves under cyclic load. Zhao et al. [30] conducted a series of experiments on the connection performance of grouting sleeves under large-strain cyclic loading, and derived formulas for estimating energy absorption and effective friction coefficients based on cumulative slip distance, grouting length and prestress. Zheng et al. [31] carried out large-deformation repeated tension and compression tests on a defective grouting sleeve, and found that when the anchorage length of the steel bars was five times the diameter, the fracture failure of the steel bars occurred. In order to study the connection performance of grouting sleeves under the combined action of an earthquake and fire, Liu et al. [32,33] carried out large-deformation repeated tension and compression tests on grouting sleeves with insufficient grouting materials in both room-temperature and high-temperature environments.

It can be observed that there is relatively limited research on the tensile performance of seamless steel pipe grouting sleeves under fire and cyclic loading conditions. Therefore, this study aims to investigate the influence of temperature and cyclic loading on the bond mechanical performance of seamless steel pipe grouting sleeves, providing insights for the design of prefabricated buildings in fire protection and cyclic loading scenarios. Three key influencing parameters are considered in this study, namely the steel bar diameter, the presence of a specimen protective layer, and the cooling method, to examine their effects on the bond performance of test pieces after exposure to high temperatures.

2. Experimental Program

2.1. Test Piece Preparation

Twenty-eight seamless steel pipe grouting sleeve connectors were made. The sleeve body was made from Q345-type seamless steel pipe material (Figure 2a). As shown in Figure 3, the outer diameter of the sleeve D_d was 45 mm, the inner diameter D was 37 mm, the thickness t was 4 mm, the rib width a was 8.0 mm, the rib spacing b was 25 mm, and the rib depth c was 1.5 mm. L was the length of sleeve. The anchorage length of every test piece was taken as $7d$. The geometric parameters of test pieces with different diameters are shown in Table 1. Test piece sets were numbered according to the following criteria: “protective layer thickness—cooling method—connection steel bar diameter—heating temperature”. As shown in Figure 2b, C0 and C20 represent grouting layer thicknesses of 0 mm and 20 mm. N and W represent natural cooling and water cooling, respectively. d18, d20 and d22 represent diameters of the connecting steel bars of 18 mm, 20 mm and 22 mm. The grouping of the test pieces and the experimental procedures are shown in Table 2. Eighteen grouting material blocks with a volume of 40 mm × 40 mm × 160 mm were also prepared to further understand the effect of grouting materials’ compressive performance deterioration on the grouting sleeve’s mechanical properties after high temperature.

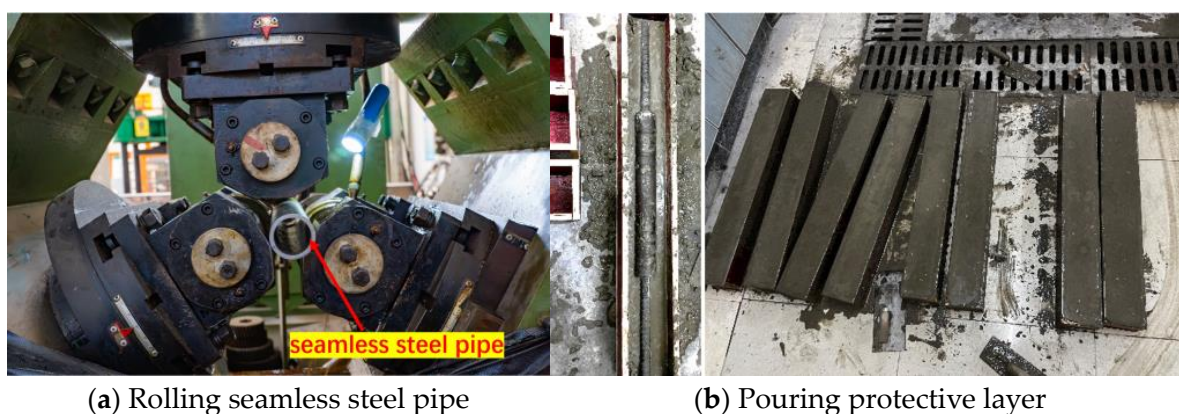


Figure 2. Test piece production.

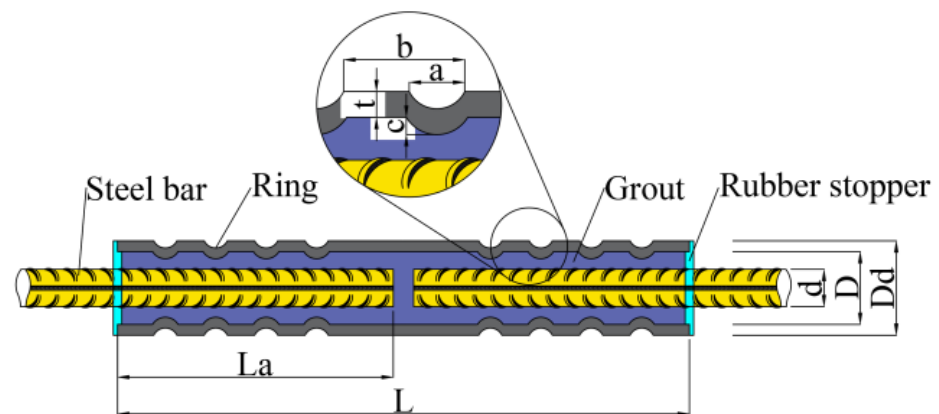


Figure 3. Seamless steel pipe grouting sleeves.

Table 1. Test piece set geometrical parameters.

Test Piece Number	d (mm)	a (mm)	L_a (mm)	L (mm)
C20-N-d18	18	1.5	126	312
C0-N-d20	20	1.5	140	340
C20-N-d20				
C20-W-d20				
C20-N-d22	22	1.5	154	368

Table 2. Main parameters of test pieces.

Group	Test Piece Number	Protective Layer (mm)	Cooling Method	Temperature (°C)
1	C0-N-d20-200 °C/400 °C/600 °C/800 °C/1000 °C	0	Natural cooling	20/200/ 400/600/ 800/1000 *
2	C20-N-d18-20 °C/200 °C/400 °C/600 °C/800 °C/1000 °C	20		
3	C20-N-d20-20 °C/200 °C/400 °C/600 °C/800 °C/1000 °C			
4	C20-N-d22-20 °C/200 °C/400 °C/600 °C/800 °C/1000 °C	20	Water cooling	800/1000 *
5	C20-W-d20-200 °C/400 °C/600 °C/800 °C/1000 °C			

* Group 1 and group 2 did not undergo 20 °C testing.

2.2. Materials

The test pieces are primarily composed of three materials: HRB400 ribbed steel bars, seamless steel pipes and grouting materials.

HRB400 ribbed steel bars are used for the connecting steel bars, and their actual yield stress and tensile strength are 485.20 MPa and 671.62 MPa, respectively. The sleeve was made from Q345 precision seamless steel tubes with a measured ultimate tensile strength of 490 MPa. All performance parameters met the requirements of the specification JGT 398-2019 [34]. The average compressive strength of the grouting material was measured to be 102.3 MPa, meeting the requirements of GB/T 17671-2021 [35].

2.3. Design of Experiments

2.3.1. Heating and Cooling Programs

The heating equipment used in this experiment was a multi-functional experimental furnace, as shown in Figure 4, and the test pieces were heated according to the standard curve defined in ISO-834 [36,37]. The heating curve is shown in Figure 5.



Figure 4. High-temperature experimental furnace.

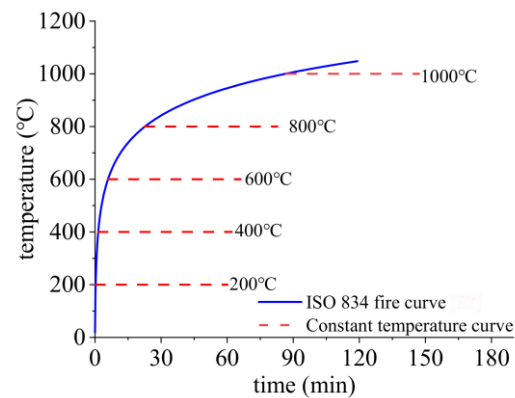


Figure 5. Rising and constant temperature curve [37].

After the test pieces were heated to the preset temperature, the temperature was kept stable for 60 min, and then the heating was stopped. Then, the naturally cooled test pieces were placed directly into a 20 °C environment, while the water-cooled test pieces were cooled with running water for 20 min immediately after removal from the furnace. Then, the concrete protective layer was broken and we removed the test pieces, as shown in Figure 6.

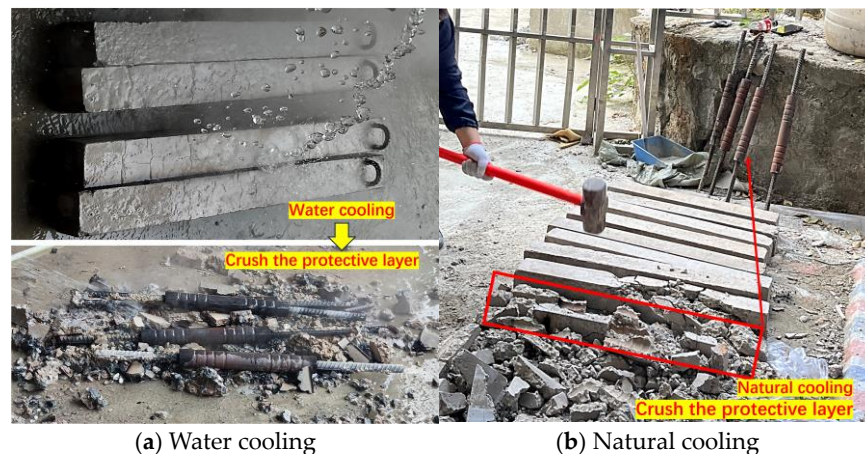


Figure 6. Cooling method of test pieces after exposure to a high temperature.

2.3.2. Loading Program

The loading test was carried out with a high-speed press testing machine (Figure 7) with a maximum static test force of 2000 kN, which can be loaded by means of force and displacement control. In this test, both the forward and the reverse loading were controlled

by the displacement, and the loading rate was 10 mm/min. The forward and reverse unloading was controlled by the force, and the unloading rate was 50 MPa/s. According to JGJ 107-2016 [14], the loading program is illustrated in Figure 8.



Figure 7. Test loading machine.

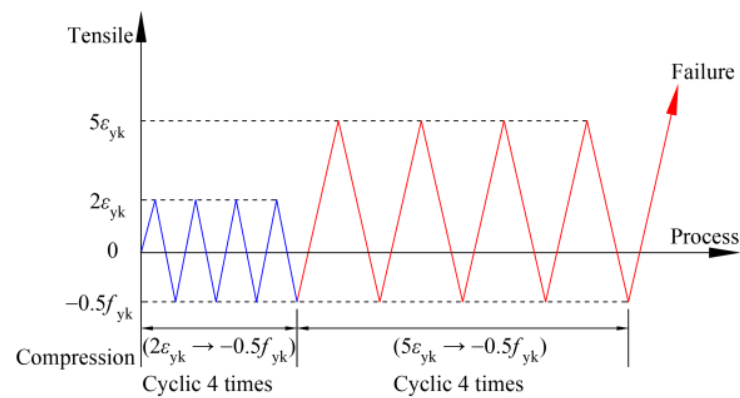


Figure 8. Loading procedure.

2.3.3. Test Methods

The load–displacement curve, ultimate load, and ultimate displacement of the test pieces were obtained as follows. Three axial strain gauges, Z1, Z2, and Z3, and three annular strain gauges, H1, H2, and H3, on the surface of the test pieces were used to measure the strain change trend of the sleeve surface. The locations of the axial and annular strain gauges are shown in Figure 9.

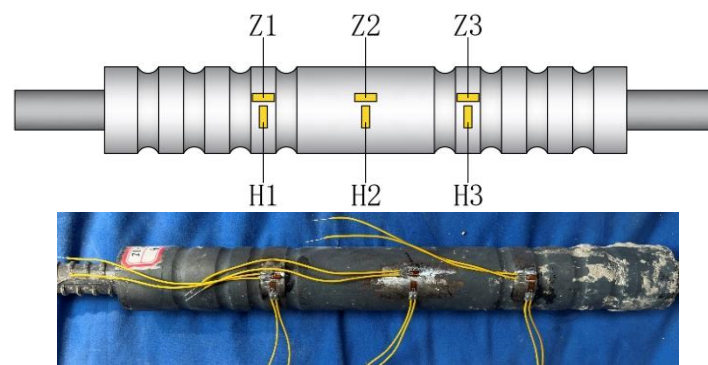


Figure 9. Strain gauges on the surface of the sleeve.

3. Experimental Results Analysis

3.1. Grouting Sleeve Test Results

3.1.1. Failure Modes

Two modes of failure appeared in the test pieces: (a) Break failure of the steel bar. As shown in Figure 10a, the bond strength of the grouting materials to the steel bar was greater than the ultimate tensile strength of the steel bar. (b) Pull-out failure. As shown in Figure 10b, the bond strength of the grouting materials to the steel bar was less than the ultimate tensile strength of the steel bar, and the steel bar pulled out of the grouting materials.

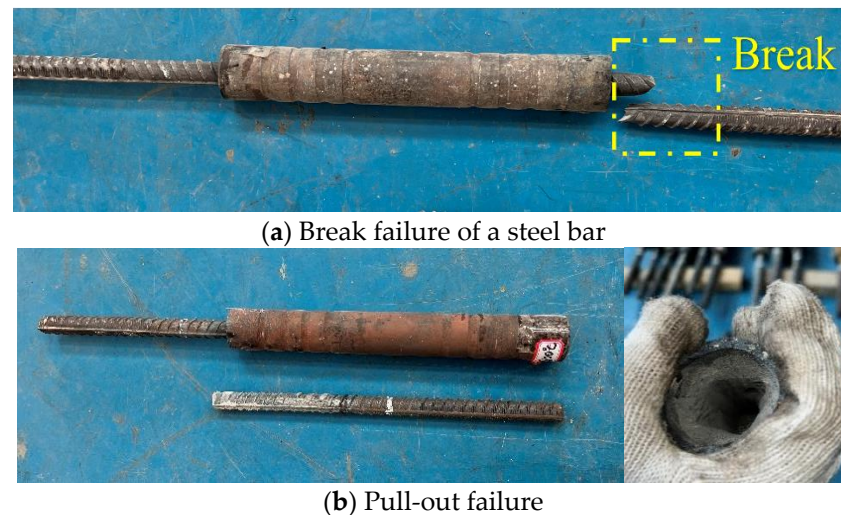


Figure 10. Test piece failure modes.

Table 3 shows the test results and failure modes of the test pieces after high temperature. After the temperature is between 20 and 600 °C, all test pieces are fractured by the breaking of the steel bars. After the temperature is 800 °C, C20-N-d18–800 °C, C20-N-d20–800 °C, and C0-N-d22–800 °C are broken by the tensile failure of the steel bars. C0-N-d20–800 °C and C20-W-d20–800 °C are fractured by the pullout failure of the steel bars. At 1000 °C, due to the significant damage caused to the bond between the grouting materials and the steel bars, all test pieces are fractured by the pull-out failure of the steel bars.

Table 3. Experimental results of test pieces.

Test Piece Number *	F_u (kN)	δ_u (mm)	f_u (Mpa)	Failure Modes
C20-N-d18–20 °C	156.55	37.96	615.51	Break
C20-N-d20–20 °C	202.42	35.61	644.65	Break
C20-N-d22–20 °C	246.96	38.07	650.00	Break
C0-N-d20–200 °C	202.41	34.14	644.62	Break
C20-N-d18–200 °C	158.40	35.18	622.79	Break
C20-N-d20–200 °C	200.29	36.75	644.24	Break
C20-N-d22–200 °C	247.93	39.33	652.55	Break
C20-W-d20–200 °C	195.33	37.28	622.07	Break
C0-N-d20–400 °C	202.84	44.19	645.99	Break
C20-N-d18–400 °C	160.76	32.45	632.07	Break
C20-N-d20–400 °C	202.42	33.79	644.65	Break
C20-N-d22–400 °C	240.71	42.25	633.55	Break
C20-W-d20–400 °C	202.91	34.53	646.21	Break

Table 3. Cont.

Test Piece Number *	F_u (kN)	δ_u (mm)	f_u (Mpa)	Failure Modes
C0-N-d20–600 °C	200.75	43.11	639.33	Break
C20-N-d18–600 °C	159.01	32.55	625.19	Break
C20-N-d20–600 °C	196.50	32.52	625.80	Break
C20-N-d22–600 °C	246.44	38.50	648.63	Break
C20-W-d20–600 °C	197.08	41.07	627.64	Break
C0-N-d20–800 °C	190.08	30.12	605.35	Pull-out
C20-N-d18–800 °C	161.47	32.71	634.86	Break
C20-N-d20–800 °C	205.20	36.22	653.50	Break
C20-N-d22–800 °C	249.57	35.15	656.87	Break
C20-W-d20–800 °C	203.47	35.49	647.99	Pull-out
C0-N-d20–1000 °C	121.87	3.10	388.12	Pull-out
C20-N-d18–1000 °C	107.82	9.03	423.92	Pull-out
C20-N-d20–1000 °C	139.75	8.89	445.06	Pull-out
C20-N-d22–1000 °C	164.76	10.15	433.65	Pull-out
C20-W-d20–1000 °C	137.55	8.80	438.05	Pull-out

* C0-N-d20–20 °C and C20-W-d20–20 °C both use the same data as the experimental results of C20-N-d20–20 °C.

3.1.2. Maximum Tensile Force

Figure 11 depicts the relationship between the ultimate tensile strength of the test piece and the temperature, compiled from the data in Table 3. After the temperature ranges from 20 to 600 °C, the group 2 test pieces show the lowest ultimate tensile strength at each temperature interval. The other four groups of test pieces did not show significant differences. After 800 °C, the test pieces belonging to group 1 and group 2 had a lower ultimate tensile strength compared to the other three groups due to steel bar pull-out failure. It is worth noting that, based on the observations at 20–800 °C, the ultimate tensile strength of all test pieces exceeded 600 MPa. At 1000 °C, all test pieces experienced steel bar pull-out failure, and compared to the 20 °C environment, the bonding performance decreased by 33.7~42.2%.

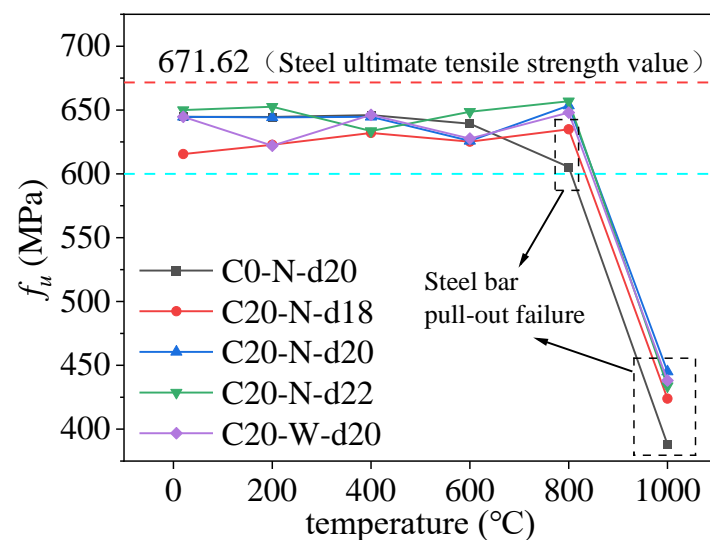


Figure 11. Relationship between the tensile strength and temperature.

It can be concluded that the test pieces with a diameter of 18 mm (group 2) showed poorer tensile performance after high temperature. There were no significant differences observed among test pieces subjected to different cooling methods at various temperatures. However, test pieces without protective layers showed inferior tensile performance compared to those with protective layers at temperatures above 800 °C.

3.1.3. Load–Displacement Curves

Figure 12 shows the load–displacement curves of the test pieces under different temperature conditions. In Figure 12a–f, it is visually evident that test pieces with larger diameters show a higher ultimate tensile strength under high temperatures. To provide a clear comparison of the effects of cooling methods and protective layers on the test pieces, only the group 1, group 3, and group 5 test pieces will be discussed.

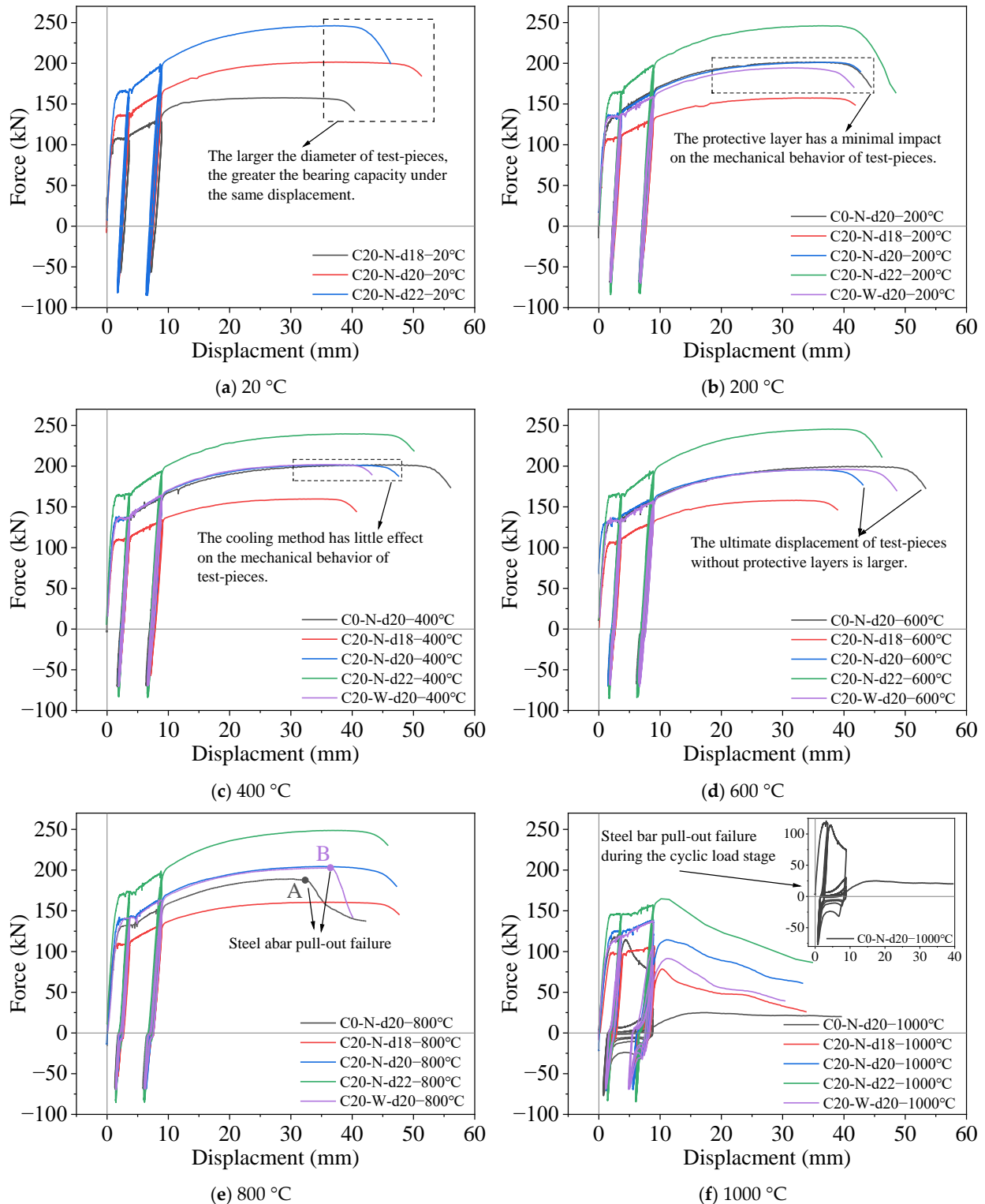


Figure 12. Load–displacement curves of test pieces.

After 200 °C (Figure 12b), compared to those subjected to natural cooling (C20-N-d20–200 °C), the water-cooled test pieces (C20-W-d20–200 °C) showed larger displacements under the same tensile force and reached the load limit earlier. The curves of C20-N-d20–200 °C and C0-N-d20–200 °C overlap almost entirely, indicating that the protective layer has minimal influence on the mechanical behavior of the test pieces at 200 °C.

After 400 °C (Figure 12c), there is little difference in the ultimate tensile strength between test pieces subjected to different cooling methods. However, the water-cooled test pieces reached the load limit earlier and showed less deformation capacity. Comparing the curves of C20-N-d20–400 °C and C0-N-d20–400 °C, it is evident that test pieces without protective layers experience significantly larger displacements.

After 600 °C (Figure 12d), the displacement of C20-W-d20–600 °C during the ultimate tensile stage is 26.29% greater than that of C20-N-d20–600 °C. This indicates that at 600 °C, compared to natural cooling, test pieces cooled by water show more significant deformation under the same load. Test pieces without protective layers also experience larger displacements.

After 800 °C (Figure 12e), C0-N-d20–800 °C and C20-W-d20–800 °C experience a sudden decrease in tension at points A and B during the ultimate tensile stage, indicating a rupture of the bond between the grout material and the connecting steel bars under tension. This results in steel bar pull-out failure. Compared to C20-N-d20–800 °C, C0-N-d20–800 °C shows larger displacement under the same tension. The ultimate tensile strength of C20-N-d20–800 °C is 205.2 kN, which is 0.85% higher than that of C20-W-d20–800 °C and 7.95% higher than that of C0-N-d20–800 °C. This indicates that at this temperature, the bond performance of test pieces subjected to natural cooling is higher than that of test pieces subjected to water cooling, and test pieces with protective layers show better bond performance.

After the temperature reaches 1000 °C (Figure 12f), all test pieces undergo significant deformation during the cyclic loading stage, indicating that the bond strength between the grouting material and the connecting steel bars sharply decreases, leading to steel bar pull-out failure in the test piece. A comparison of test pieces with different diameters of the connecting steel bars reveals that the ultimate tensile force of C20-N-d22–1000 °C is 17.83% greater than that of C20-N-d20–1000 °C and 52.73% greater than that of C20-N-d18–1000 °C, indicating that test pieces with larger connecting steel bar diameters show better bonding strength. Test pieces subjected to natural cooling show a tensile strength during the tensile stage that is 24.9% higher than those subjected to water cooling. Due to the test piece not having a protective layer, C0-N-d20–1000 °C experiences nonlinear changes in its load–displacement curve during the cyclic loading stage. Moreover, as the number of cycles increases, damage accumulates in the grout under the compression of the connecting steel bar ribs, eventually leading to steel bar pull-out failure in this test piece.

It can be concluded that test pieces with larger steel bar diameters show better tensile performance at different high temperatures. Cooling methods have a minimal impact on the bond performance of test pieces at temperatures below 600 °C, but at 800–1000 °C, test pieces subjected to natural cooling show better bond performance. Test pieces with protective layers experience smaller ultimate displacements under large-strain cyclic loading, while those without protective layers show greater deformation.

3.1.4. Load–Strain Curves

The performance of the load–strain curves of test pieces under different temperature conditions can be observed in Figures 13–17. When subjected to tension, the axial strains Z1, Z2, and Z3 on the outer wall of the sleeve are greater than 0, while the circumferential strains H1, H2, and H3 are less than 0, indicating that the sleeve is under axial tension and circumferential compression. The maximum tensile strain and maximum compressive strain for each test piece both occur at measurement points Z2 and H2. The maximum circumferential strain and axial strain measured during the experiment are -468.98×10^{-6} and 1298.23×10^{-6} , respectively. During the large-deformation repeated tension and

compression period, the “coincidence” of the load–strain curves under compression force is better than that under tension force, because the compressive strength of the grouting materials is greater than its tensile strength.

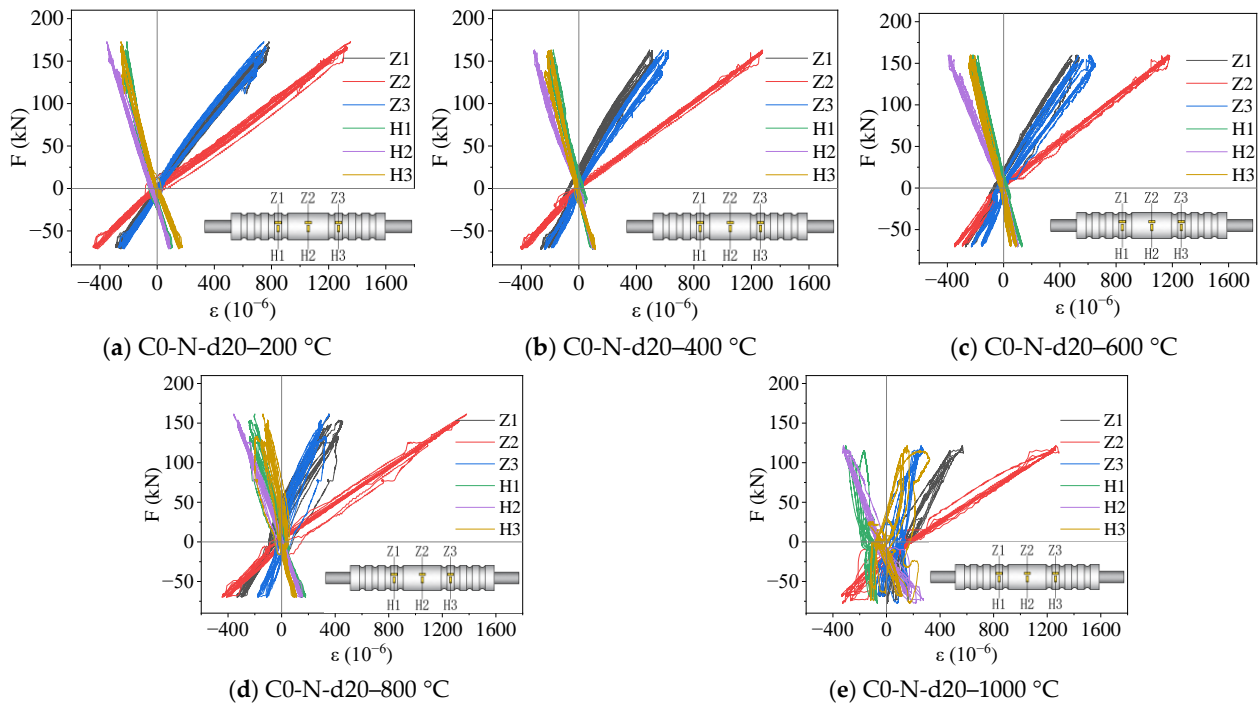


Figure 13. Load–strain curves of group 1 test pieces.

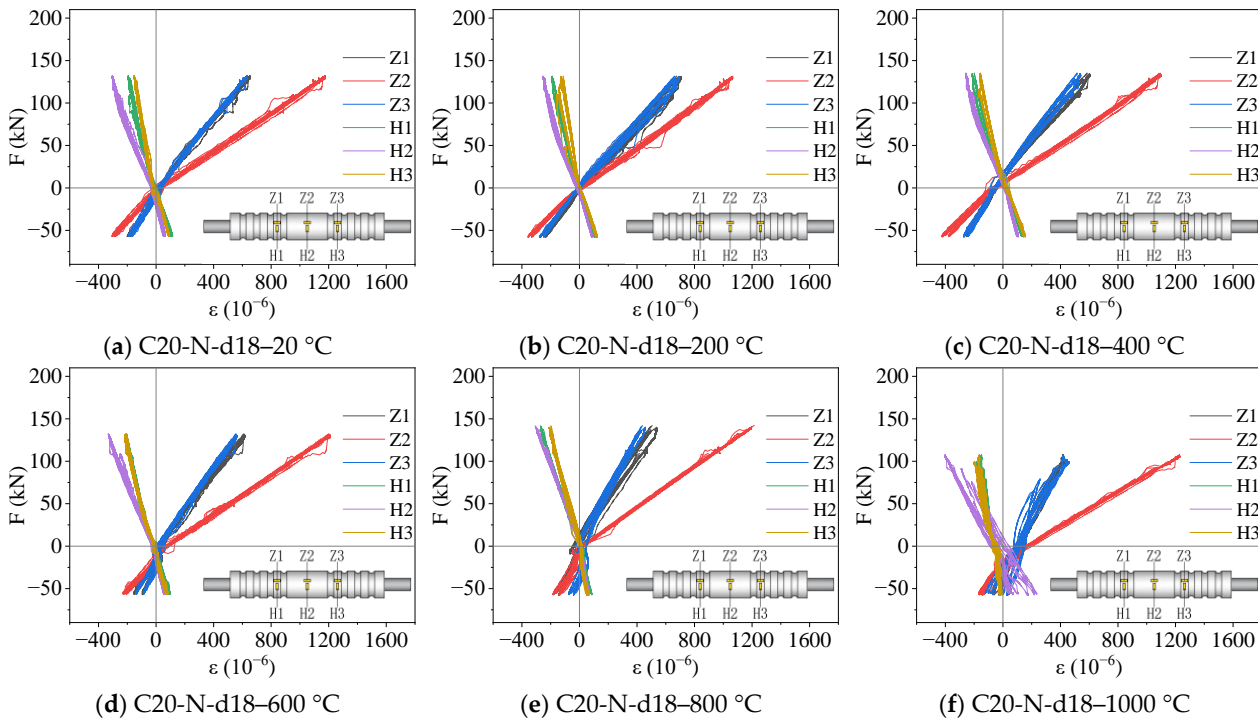


Figure 14. Load–strain curves of group 2 test pieces.

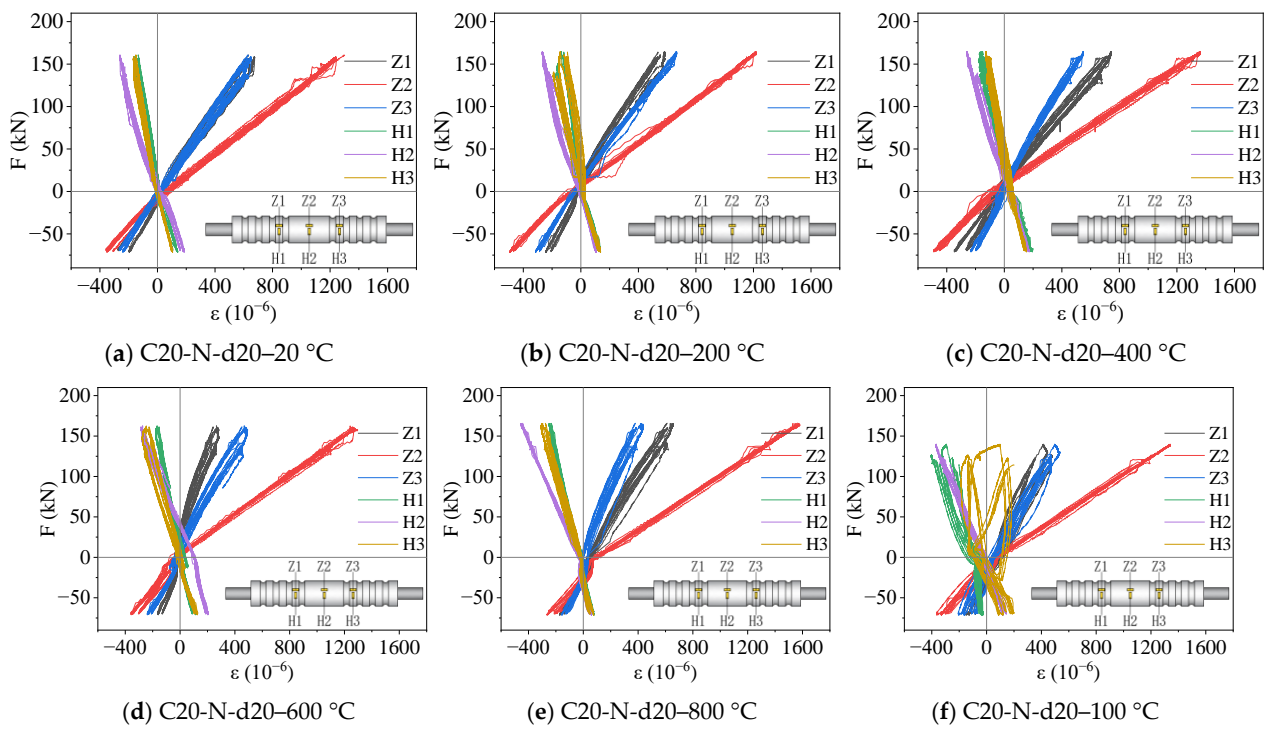


Figure 15. Load-strain curves of group 3 test pieces.

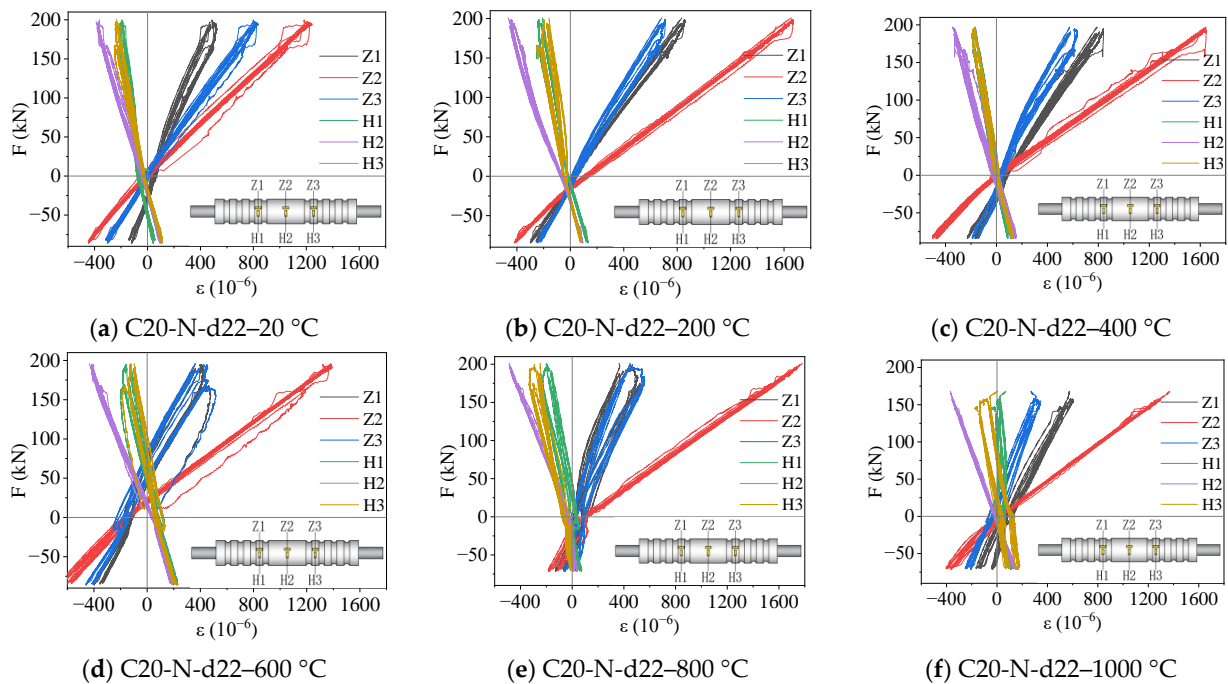


Figure 16. Load-strain curves of group 4 test pieces.

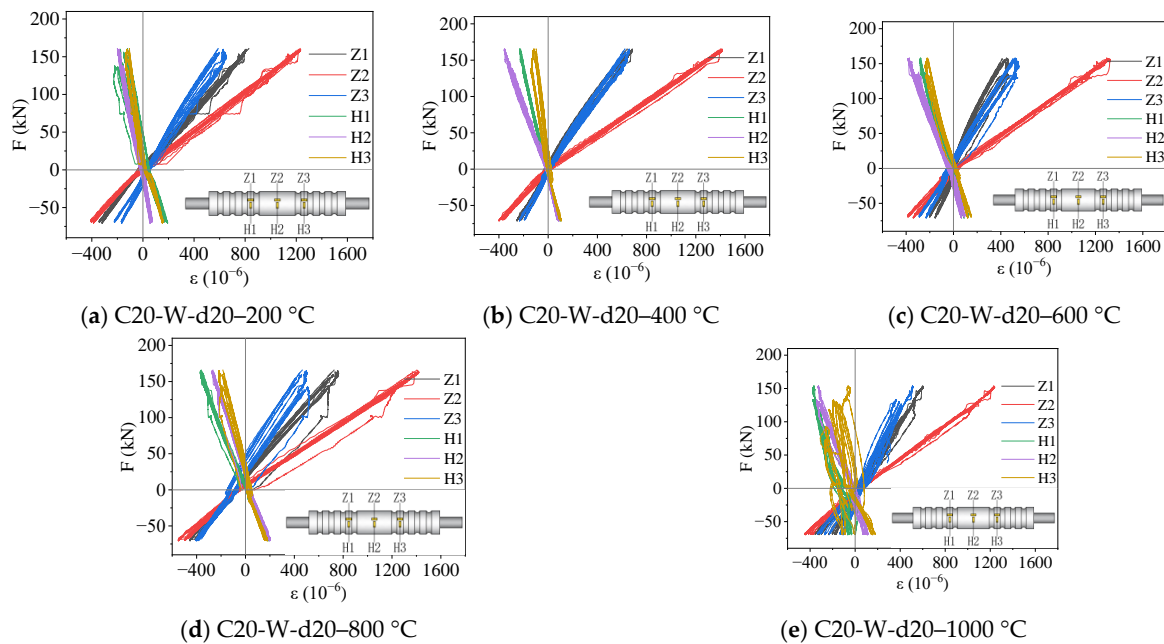


Figure 17. Load–strain curves of group 5 test pieces.

Comparing the strain variations of the test pieces at different temperatures, taking the first group of test pieces as an example, it is observed that as the temperature increases, the “overlap” of the curves gradually decreases. Moreover, the overlap at the central measurement points Z2 and H2 is higher than at other points, indicating significant deformation damage in the ribbed section. In Figure 13a–e, it is visually apparent that after high temperatures of 800 °C and 1000 °C, the load–strain curves of all test pieces do not overlap significantly, indicating significant damage to the test pieces’ elastic deformation performance.

Comparing test pieces with different diameters, in group 2 (Figure 14), the paths of the Z1 and Z3 curves show a high degree of similarity. However, in the group 3 (Figure 15) and group 4 (Figure 16) test pieces groups, Z1 and Z3 show significant misalignment, indicating that the deformations of the test pieces with connecting steel bars belonging to group 2 are more uniform under high temperatures. In group 4 test pieces, as the temperature increases, the increment of strain values at measurement points Z1, Z3, H1, and H3 in the second cycle is greater than that in the first cycle, leading to an increase in residual strain. This suggests that in test pieces with larger steel bar diameters at high temperatures, the bond between the steel bars and the grout surface at the ribs is severely damaged.

Comparing test pieces subjected to different cooling methods, belonging to group 3 and group 5 (Figure 17), after temperatures ranging from 20 to 600 °C, test pieces subjected to different cooling methods did not show significant differences. However, at temperatures of 800 °C and 1000 °C, the alignment of the Z1, Z2, and Z3 curves in the group 3 test pieces was better than that in the group 5 test pieces. This indicates that after experiencing temperatures higher than 800 °C, test pieces subjected to natural cooling demonstrate better elasticity under cyclic loading.

Comparing test pieces with and without protective layers, belonging to group 1 (Figure 13) and group 3, test pieces with protective layers show better curve alignment at high temperatures compared to test pieces without protective layers, indicating that a protective layer provides better preservation of the test pieces’ elasticity under high-temperature conditions.

In summary, as the temperature rises, the magnitude of deformation damage to the outer wall of the sleeve increases, especially in the ribbed section. Test pieces with larger steel bar diameters show more severe damage to the ribs. Regarding the effects of cooling methods and protective layers, adopting natural cooling or having protective layers is beneficial in reducing deformation damage to the test pieces.

3.2. Grouting Materials' Performance Deterioration Analysis

3.2.1. High Temperature Effects

This article conducted compressive strength tests on 18 grouting material blocks. Figure 18 illustrates the relationship between the compressive strength of these grouting material blocks and temperature. After 600 °C, the compressive strength is 83.1 MPa, 15.98% lower than that at 20 °C. However, after the temperature reaches 600–1000 °C, the loss of compressive strength becomes larger. When the temperature reaches 1000 °C, the compressive strength of the grouting materials is only 27.50% of that at 20 °C, and the compressive performance is essentially lost.

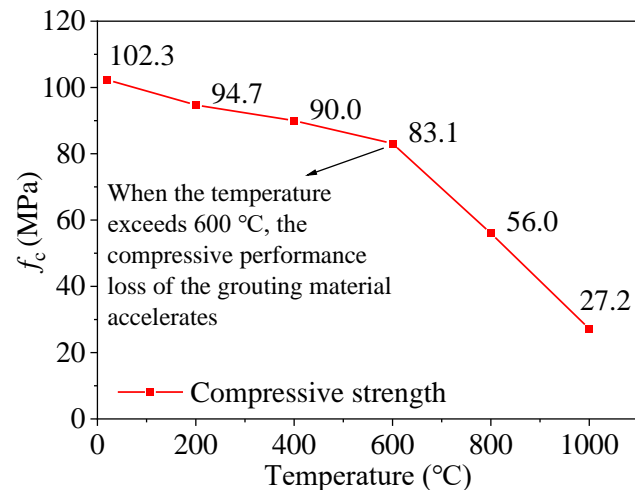


Figure 18. Compressive strength of grouting material blocks at different temperatures.

3.2.2. Apparent Deterioration of Grouting Materials

To further investigate the effect of temperature on the grouting materials of the sleeve, C0-N-d20–600 °C and C0-N-d20–800 °C test pieces were subjected to cut analysis (Figure 19). The observations reveal that grout cracks are mainly concentrated near the ribs, with significant lateral cracks in this area accompanied by a small amount of debris. This indicates that under cyclic loading, the ribs restrict the cyclic sliding of the grouting materials, leading to extrusion of the grout. At the end of the sleeve, as shown in region A of Figure 19, there are more cracks and greater fragmentation of the grouting materials. Additionally, due to the lack of rib constraints, the grouting materials are pulled out along with the steel bars.

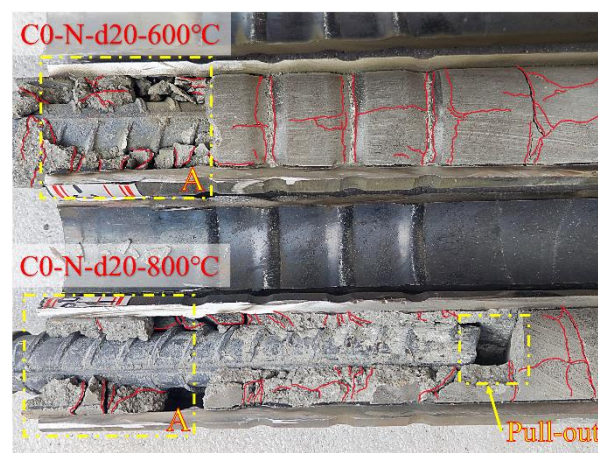


Figure 19. Cutting of test pieces and crack distribution.

Figure 20 shows the local force model of the grouting materials in the grouting sleeve when it is under tension. The grouting materials are in a state of compression due to the constraints of the sleeve ring rib and the ribbed connecting steel bars during the cyclic load of the grouting sleeve.

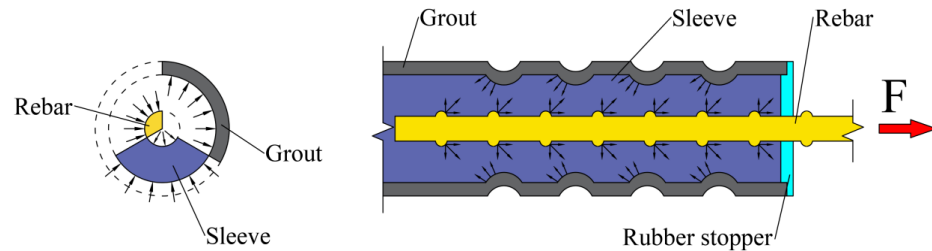


Figure 20. Local force model of the grouting materials of the grouting sleeve under tension.

3.2.3. Microscopic Analysis of Grouting Materials' Deterioration

The test pieces belonging to group 2 were sampled, and the internal structure of the grouting materials was magnified by 5000 times with SEM. The results are shown in Figure 21. After 20 °C (Figure 21a), calcium hydroxide (C-H) and calcium silicate hydrate (C-S-H) show good adhesion to the aggregate surface, forming a continuous phase through the mutual bonding of hydration products, resulting in fewer voids.

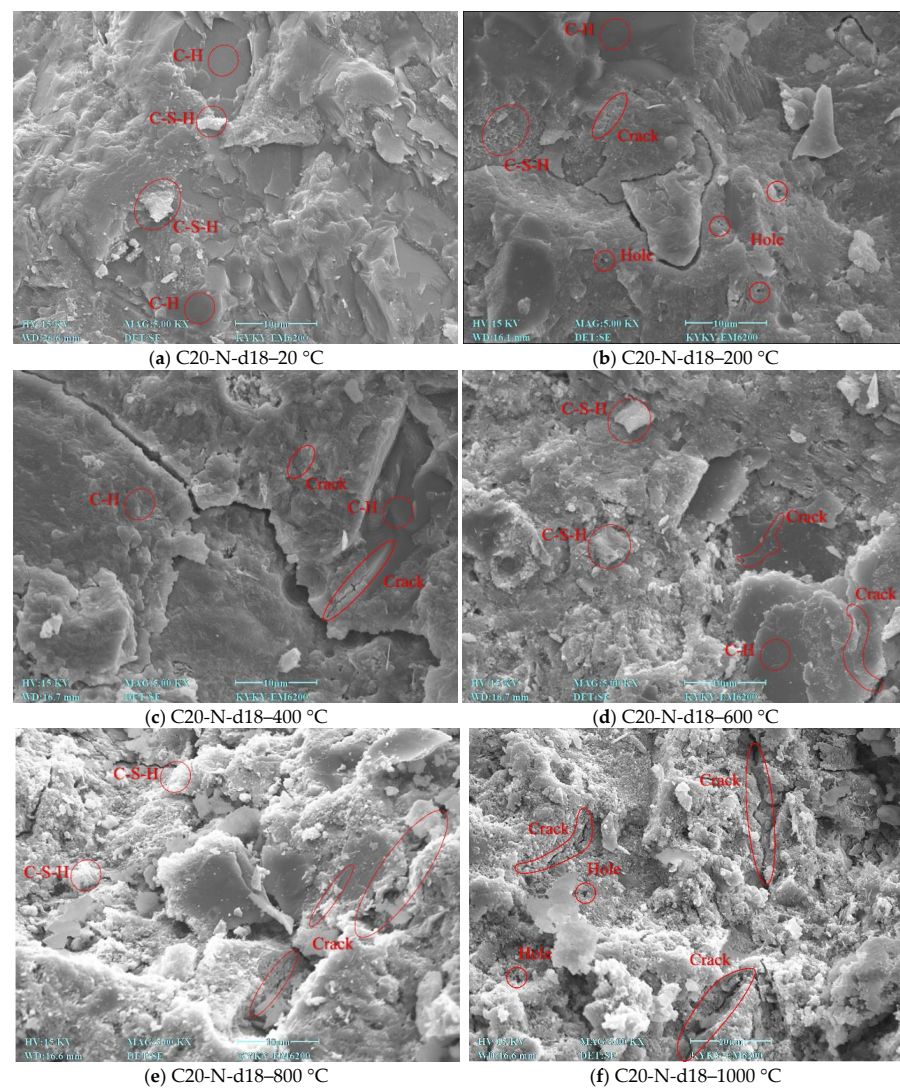


Figure 21. SEM scanning results of the grouting materials belonging to group 2.

After 200 °C, the test pieces display the evaporation of capillary water and gel water. Microscopically, small pores can be observed (Figure 21b), but the overall structure remains largely unchanged compared to that at 20 °C ambient conditions. The grouting materials structure appears relatively dense, with good bonding of C-H crystals.

After 400 °C, as shown in Figure 21c, in addition to the evaporation of capillary water and gel water within the grouting materials, some crystalline hydrates begin to lose water molecules. The decomposition of C-H crystals becomes apparent, accompanied by the emergence of noticeable pores on the surface. Consequently, cracks further propagate, and the density of hydration products significantly decreases.

After reaching 600 °C (Figure 21d), further decomposition of C-H occurs, resulting in the appearance of unevenly sized crystalline particles and increased porosity. Cracks become more prominent, but there is no apparent complete penetration of cracks. The degradation of mechanical properties is relatively minor.

After the temperature reaches 800 °C (Figure 21e), C-S-H begins to decompose, with severe dehydration of structural water. Dispersed particles appear inside the grouting materials, and numerous interconnected microcracks emerge on the aggregate surface. Continuous or large pieces of hydrated cementitious gel are no longer present within the concrete. The overall structure of the grouting materials becomes loose and crumbly.

After exposure to a temperature of 1000 °C (Figure 21f), C-S-H is essentially completely decomposed, and CaCO₃ begins to decompose under high-temperature conditions. Structural water undergoes extensive dehydration, resulting in a significant increase in internal pores. Large gaps and cracks appear between the aggregates, exacerbating the looseness of the grouting materials. Macroscopically, there is a sharp decline in mechanical performance. Comparing the SEM scanning results of the grouting materials after subjecting them to different temperatures, it can be seen that the deterioration degree of the grouting materials' microstructure changes significantly from 600 °C to 800 °C and then 1000 °C, which corresponds to the compressive strength curve of the grouting materials after different high temperatures (Figure 18).

4. Grouting Sleeve Performance Analysis

4.1. Joint Grade

According to the provisions of JGJ 107-2016 [14], Table 4 lists the residual deformation grades of the test pieces. The ultimate tensile strength of steel joints is divided into three classes: class I, class II and class III. As Table 3 shows, the ultimate tensile strength of all test pieces is greater than $1.10f_{stk} = 594$ MPa between temperatures of 20 and 600 °C, meeting the standards of class I joints. After exposure to a temperature of 800 °C, for C0-N-d20–800 °C and C20-W-d20–800 °C, despite the failure of steel bar pull-out, their ultimate tensile strength is still greater than $1.10f_{stk}$, meeting the standards of class I joints. That is, after 800 °C, all test pieces still meet the class I joint standards. After the temperature reaches 1000 °C, the standard tensile strength of all test pieces is lower than $1.25f_{yk} = 500$ MPa, which means that all test pieces cannot meet the requirements of class III joint standards.

Table 4. Performance grade of the test pieces.

Class of Test Pieces	I	II	III
Ultimate tensile strength	$f_{mst}^0 \geq f_{stk}$ Bar breaking, or $f_{mst}^0 \geq 1.10f_{stk}$ Pull-out failure	$f_{mst}^0 \geq 1.10f_{stk}$	$f_{mst}^0 \geq 1.25f_{yk}$
large strain of cyclic loading	$u_4 \leq 0.3$ and $u_8 \leq 0.6$		$u_4 \leq 0.6$

4.2. Residual Deformation

Residual deformation is one of the most important indicators used to evaluate the recoverability of grouting sleeves under cyclic loading. According to the specification of JGJ107-2016 [14], the requirements for large-deformation repeated tension and compression

stipulate that $u_4 \leq 0.3$ mm and $u_8 \leq 0.6$ mm. The calculations of u_4 and u_8 are defined in Equations (1) and Equation (2) [14] and are shown in Figure 22.

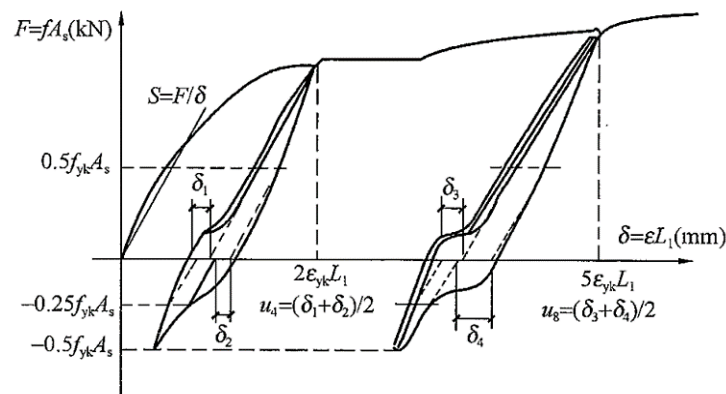


Figure 22. Residual deformation calculation parameters.

$$u_4 = \frac{\delta_1 + \delta_2}{2} \quad (1)$$

$$u_8 = \frac{\delta_3 + \delta_4}{2} \quad (2)$$

Table 3 shows the residual deformation performance of test pieces. According to Table 5, when the temperature is below 600 °C, all test pieces meet the requirements of residual deformation under repeated loads. When the temperature reaches 800 °C, for group 1, its $u_4 = 0.32 > 0.3$ and $u_8 = 0.86 > 0.6$, meaning that it does not meet the deformation performance standards of class III joints. and for group 5, its $u_4 = 0.31 > 0.3$ and $u_8 = 0.46 < 0.6$, meaning that it meets the deformation performance standards of class III joints, but does not meet the deformation performance standards of class I joints. When the temperature reaches 1000 °C, all test pieces do not meet the deformation performance standards of class III joints.

Table 5. Residual deformation performance of test pieces.

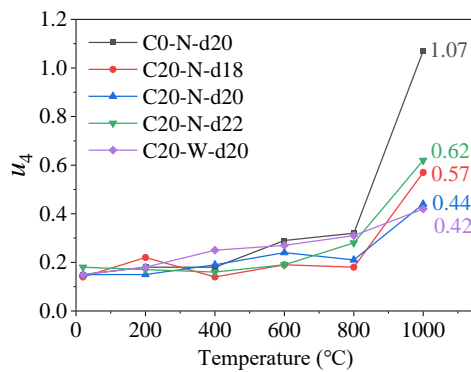
Test Piece Number	u_4 (mm)	u_8 (mm)
C20-N-d18–20 °C	0.14	0.21
C20-N-d20–20 °C	0.15	0.27
C20-N-d22–20 °C	0.18	0.26
C0-N-d20–200 °C	0.18	0.26
C20-N-d18–200 °C	0.22	0.26
C20-N-d20–200 °C	0.15	0.26
C20-N-d22–200 °C	0.17	0.25
C20-W-d20–200 °C	0.18	0.25
C0-N-d20–400 °C	0.18	0.31
C20-N-d18–400 °C	0.14	0.17
C20-N-d20–400 °C	0.19	0.43
C20-N-d22–400 °C	0.16	0.26
C20-W-d20–400 °C	0.25	0.26
C0-N-d20–600 °C	0.29	0.56
C20-N-d18–600 °C	0.19	0.21
C20-N-d20–600 °C	0.24	0.27
C20-N-d22–600 °C	0.19	0.31
C20-W-d20–600 °C	0.27	0.26

Table 5. Cont.

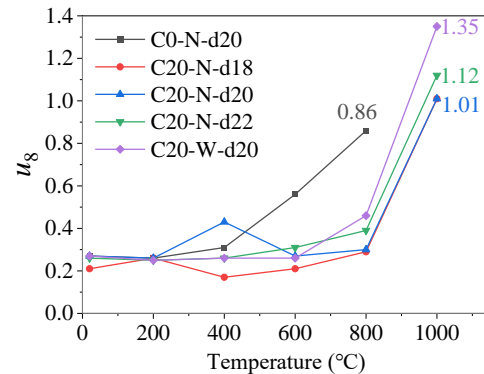
Test Piece Number	u_4 (mm)	u_8 (mm)
C0-N-d20–800 °C	0.32	0.86
C20-N-d18–800 °C	0.18	0.29
C20-N-d20–800 °C	0.21	0.3
C20-N-d22–800 °C	0.28	0.39
C20-W-d20–800 °C	0.31	0.46
C0-N-d20–1000 °C	1.07	- *
C20-N-d18–1000 °C	0.57	1.01
C20-N-d20–1000 °C	0.44	1.01
C20-N-d22–1000 °C	0.62	1.12
C20-W-d20–1000 °C	0.42	1.35

* "-" No data, the test piece does not withstand 8 cycles of large-strain cyclic loading.

Figure 23 shows the variation trend of u_4 and u_8 of each test piece under large-strain cyclic loading. With the increase in temperature, the values of u_4 and u_8 have an overall upward trend, and as the temperature rises from 800 °C to 1000 °C, the slope of the curve increases sharply, indicating that large-deformation repeated tension and compression of the test piece occur. As shown in Figure 23a, between 400 °C and 1000 °C, both the value and the slope of group 1 are significantly larger than those of group 3. That reveals that the residual deformation u_4 of the test pieces without a protective layer is more obvious, so the protective layer can effectively reduce the mechanical loss of the grouting sleeve after exposure to a high temperature. In Figure 23b, the difference in the u_8 between group 3 and group 5 is 0.16 after 800 °C, but after 1000 °C, this value becomes 0.34, an increase of 112.50%. In other words, group 5 has a larger residual deformation at a higher temperature, which indicates that with the increase in the number of cycles, the grouting materials of the water-cooled test pieces are more seriously damaged after 1000 °C.



(a) Residual deformation after 4 cycles



(b) Residual deformation after 8 cycles

Figure 23. The residual deformation of test pieces under large-deformation repeated tension and compression.

Figure 24 shows the difference between u_8 and u_4 (i.e., D-value), and also displays the second half of the residual deformation of the test pieces under large-strain cyclic loading. After the temperature is 800 °C, C0-N-d20–800 °C experiences steel bar pull-out failure, and its D-value is 0.54. When the temperature is 1000 °C, all the test pieces experience steel bars pull-out failure, and the D-value of C20-N-d18–1000 °C is the lowest, at 0.44. Based on the data above, to avoid steel bar pull-out failure, a safety D-value of 0.27 is recommended when fire and seismic design is performed for seamless steel pipe grouting sleeves.

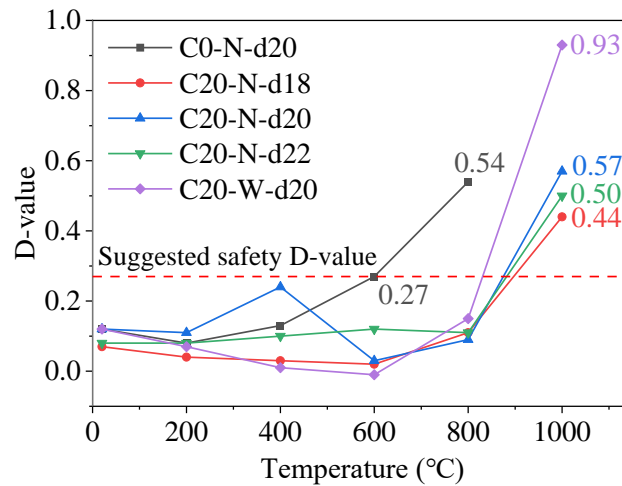


Figure 24. The difference between the u_8 and u_4 of test pieces under large-deformation repeated tension and compression.

5. Bond Stress Analysis

Regarding the bond strength between steel bars and grouting materials, Einea et al. [2] posited a correlation between the bond strength and the compressive strength of grouting materials. They defined the coefficient k as the correlation coefficient. The formulas for bond force f_c and bond strength U are as follows [2]:

$$U = \frac{F_u}{\pi d L_a} \quad (3)$$

$$U = k \sqrt{f_c} \quad (4)$$

Combining Equations (3) and (4), k is defined as

$$k = \frac{F_u}{\pi d L_a \sqrt{f_c}} \quad (5)$$

Figure 25 show the values of k for each test piece at different temperatures and their respective trends with temperature variation. In the range of 20–800 °C, the k value increases with increasing temperature. At 800 °C, the test pieces showing steel bar pull-out failure show a minimum k value of 3.03 (C20-N-d18–800 °C), while at 1000 °C, the minimum k value of 2.66 (C0-N-d20–1000 °C). Therefore, it is recommended in test piece design that the k value should not exceed 2.66.

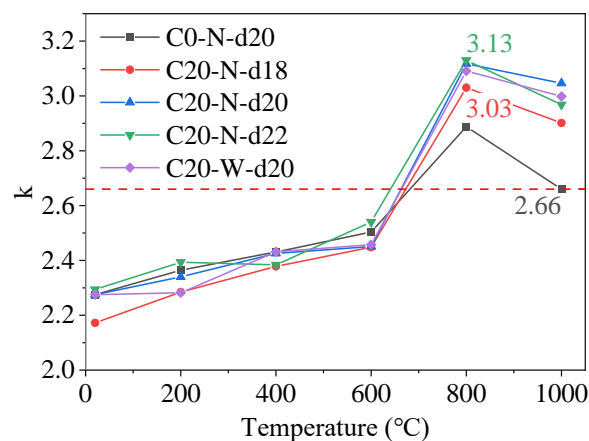


Figure 25. Calculation results of test piece k values.

Additionally, when designing test pieces, it is common practice to consider the connection steel bar's ultimate standard value as the design basis, according to the conversion formula between tensile strength (P) and tensile force (F_u):

$$P = \frac{4F_u}{\pi d^2} \quad (6)$$

When P is the standard value of ultimate tensile strength of steel bar $f_{stk} = 540$ MPa [38], combining Equations (5) and (6), the reference k for test piece design can be obtained:

$$k = \frac{f_{stk}d}{4L_a\sqrt{f_c}} \quad (7)$$

Table 6 presents the calculated results of k at different temperatures. It is evident that the value of k increases with the rise in temperature, and after 800 °C, the calculated $k = 2.58$. In the consideration of fire safety design, adjusting the anchor length L_a can influence the stability and fire resistance performance of the structure. It is recommended that practitioners control the parameter $k \leq 2.58$.

Table 6. The calculated values of k at different temperatures.

Temperature	20 °C	200 °C	400 °C	600 °C	800 °C	1000 °C
k	1.91	1.98	2.03	2.12	2.58	3.70

6. Conclusions

This study investigates the bond performance of grouting sleeves for seamless steel pipes under the effects of large-deformation repeated tension and compression after high temperature, considering the influence of steel bar diameter, cooling methods, and protective layers. Twenty-eight test pieces were designed, and the following main conclusions were drawn:

- (1) Within the temperature range of 20–800 °C, the ultimate bearing capacity of test pieces is less than 9.87% of the ultimate bearing capacity of the steel bars, with no significant decrease in bond performance. After 1000 °C, all test pieces experienced steel bar pull-out failure, with bond performance decreasing by 33.7% to 42.2%, indicating severe damage to the bond strength between the grout and steel bars.
- (2) Test pieces with a 22 mm bar diameter show a higher ultimate tensile strength after exposure to high temperatures compared to those with 20 mm and 18 mm diameters, with increases of 21.6% and 54.4%, respectively. Larger bar diameters result in better connection performance.
- (3) The influence of different cooling methods on the ultimate bearing capacity of test pieces is not significant at various temperatures, with a maximum difference of only 4.96 kN.
- (4) Test pieces with protective layers show smaller deformations within the temperature range of 20–600 °C, and their bond performance improves when temperatures exceed 800 °C.
- (5) The maximum circumferential strain and maximum axial strain of the test pieces are -468.98×10^{-6} and 1298.23×10^{-6} , respectively, both indicating elastic deformation. However, with increasing temperature, the elastic deformation capacity of the test pieces gradually decreases.
- (6) The compressive strength of grout test pieces decreases slowly within the temperature range of 20–600 °C, but the rate of strength loss increases after exceeding 600 °C. After reaching 1000 °C, the compressive strength of grout test pieces is only 27.5% of that at 20 °C.

- (7) Scanning electron microscopy (SEM) analysis reveals that the decomposition of C-H and C-S-H at high temperatures is the main reason for the decrease in the compressive strength of the grout.
- (8) A correlation coefficient k between the average bond strength of the grout and its compressive strength is proposed, with a recommendation that $k \leq 2.58$ is maintained in test piece design.

These conclusions provide an important reference basis for the fire resistance performance of prefabricated buildings under fire conditions.

Author Contributions: Conceptualization, J.Z.; Methodology, C.W.; Software, J.C.; Validation, B.M. and W.X.; Formal analysis, J.C. and B.M.; Investigation, C.W. and B.M.; Resources, J.Z.; Data curation, J.C.; Writing—original draft, C.W.; Writing—review & editing, C.W. and W.X.; Visualization, W.X.; Supervision, J.Z.; Project administration, J.Z. All authors have read and agreed to the published version of the manuscript.

Funding: This research was funded by the National Natural Science Foundation of China, grant number 12162010.

Data Availability Statement: The data used to support the findings of this study are available from the corresponding authors upon request. The data are not publicly available due to privacy.

Conflicts of Interest: The authors declare no conflict of interest.

Notations

d	Diameter of connecting steel bar
L_a	Anchorage length of connecting steel bar
F_u	Maximum tensile force at the test piece failure
δ_u	Displacement of the test piece under ultimate tensile strength
f_u	The maximum tensile force at specimen failure
f_{stk}	Standard value of the ultimate tensile strength of the steel bar
f_{mst}^0	Ultimate tensile strength measured from the test piece
ε_{yk}	The strain corresponding to the yield strength standard value of the steel bar
f_{yk}	Standard value of the yield strength of the steel bar
f_c	Compressive strength of the grout
u_4	Residual deformation after 4 cycles of large-deformation repeated tension and compression
u_8	Residual deformation after 8 cycles of large-deformation repeated tension and compression
F	Force on the steel bar
δ	Deformation of the steel bar under the force
A_s	Theoretical cross-sectional area of the steel bar
L_1	Measuring distance
δ_1	The deformation value represented by the distance between the parallel line and the abscissa at the loading force of $2f_{yk}A_s$ and reverse unloading force of $-0.25f_{yk}A_s$ after repeated loading $2\varepsilon_{yk}L_1$ for 4 cycles.
δ_2	The deformation value at the unloading force of $2f_{yk}A_s$ and reverse loading force of $-0.25f_{yk}A_s$ under the same situation.
δ_3, δ_4	The deformation values obtained by the same method after repeating load of $5\varepsilon_{yk}L_1$ for 4 cycles.
U	Bond strength between steel bars and grouting materials
k	The correlation coefficient between U and $\sqrt{f_c}$

References

1. Yee, A.A. Social and environmental benefits of precast concrete technology. *PCI J.* **2001**, *46*, 14–19. [[CrossRef](#)]
2. Einea, A.; Yamane, T.; Tadros, M.K. Grout-filled pipe splices for precast concrete construction. *PCI J.* **1995**, *40*, 82–93. [[CrossRef](#)]
3. Ling, J.H.; Rahman, A.B.A.; Ibrahim, I.S.; Hamid, Z.A. Behaviour of grouted pipe splice under incremental tensile load. *Constr. Build. Mater.* **2012**, *33*, 90–98. [[CrossRef](#)]
4. Hosseini, S.J.A.; Rahman, A.B.A.; Baharuddin, A. Analysis of spiral reinforcement in grouted pipe splice connectors. *Gradjevinar* **2013**, *65*, 537–546.

5. Alias, A.; Zubir, M.A.; Shahid, K.A.; Rahman, A.B.A. Structural performance of grouted sleeve connectors with and without transverse reinforcement for precast concrete structure. *Procedia Eng.* **2013**, *53*, 116–123. [[CrossRef](#)]
6. Alias, A.; Sapawi, F.; Kusbiantoro, A.; Zubir, M.; Rahman, A.A. Performance of grouted splice sleeve connector under tensile load. *J. Mech. Eng. Sci.* **2014**, *7*, 1094–1102. [[CrossRef](#)]
7. Harajli, M.H.; Hout, M.; Jalkh, W. Local bond stress-slip behavior of reinforcing bars embedded in plain and fiber concrete. *Mater. J.* **1995**, *92*, 343–353.
8. Haber, Z.B.; Saiidi, M.S.; Sanders, D.H. Behavior and simplified modeling of mechanical reinforcing bar splices. *ACI Struct. J.* **2015**, *112*, 179. [[CrossRef](#)]
9. Haber, Z.B.; Saiidi, M.S.; Sanders, D.H. Seismic performance of precast columns with mechanically spliced column-footing connections. *ACI Struct. J.* **2014**, *111*, 639–650. [[CrossRef](#)]
10. Shakir, Q.M.; Hamad, S.A. Behavior of pocket-type high-strength RC beams without or with dapped ends. *Pract. Period. Struct. Des. Constr.* **2021**, *26*, 04021048. [[CrossRef](#)]
11. Shakir, Q.M.; Hamad, S.A. Enhancement of the behaviour of reinforced concrete dapped end beams including single-pocket loaded by a vertical concentrated force. *Eng. Rev.* **2023**, *43*, 29–48. [[CrossRef](#)]
12. Southeast University. A Kind of Grouting Sleeve for Rebar Slurry Anchor Butt-Joint. Connection. Patent CN201320407071.4, 15 January 2014.
13. Zheng, Y.; Guo, Z.; Cao, J. Confinement mechanism and confining stress distribution of new grouting coupler for rebars splicing. *J. Harbin Inst. Technol.* **2015**, *47*, 106–111.
14. JGJ 107-2016; Technical Specification for Mechanical Splicing of Steel Reinforcing Bar. China Architecture & Building Press: Beijing, China, 2016.
15. National Fire and Rescue Administration. National Alarms and Fires 2022 [EB/OL]. (24 March 2023). Available online: <https://www.119.gov.cn/qmxfwx/xfyw/2023/36210.shtml> (accessed on 9 June 2023).
16. Zhao, X.L.; Ghojel, J.; Grundy, P.; Han, L. Behaviour of grouted sleeve connections at elevated temperatures. *Thin-Walled Struct.* **2006**, *44*, 751–758. [[CrossRef](#)]
17. Xiao, J.; Liu, L.; Ding, T.; Xie, Q. Experimental study on mechanical behavior of thermally damaged grouted sleeve splice under cyclic loading. *Struct. Concr.* **2020**, *21*, 2494–2514. [[CrossRef](#)]
18. Liu, L.; Xiao, J.; Ding, T.; Zhang, L. Mechanical behaviours of heat-damaged grouted sleeve connections. *Fire Saf. J.* **2021**, *122*, 103345. [[CrossRef](#)]
19. Liu, L.; Ouyang, L.; Ouyang, X.; Li, W.; Xiao, J. Postfire Mechanical Behaviors of Grouted Sleeve Connections Under Strong Earthquakes. *Fire Technol.* **2023**, *59*, 2829–2852. [[CrossRef](#)]
20. Zhang, W.; Deng, X.; Zhang, J.; Yi, W. Tensile behavior of half grouted sleeve connection at elevated temperatures. *Constr. Build. Mater.* **2018**, *176*, 259–270. [[CrossRef](#)]
21. Zhang, W.; Lv, W.; Zhang, J.; He, C.; Deng, X.; Yi, W. Post-fire tensile properties of half-grouted sleeve connection under different cooling paths. *Fire Saf. J.* **2019**, *109*, 102848. [[CrossRef](#)]
22. Zhu, J.; Ma, J.; Guo, D.; Wu, Y.; Ma, J. Study on tensile properties of semi grouted sleeve connectors after high temperature. *Constr. Build. Mater.* **2021**, *302*, 124088. [[CrossRef](#)]
23. Zhu, J.; Guo, D.; Ma, J.; Wu, Y.; Ma, J. Experimental study on tensile properties of semi-grouting sleeve after high temperature. *Eng. Mech.* **2020**, *37*, 104–111.
24. Li, M. Experimental Research on Mechanical Properties of Semi-Grouting Sleeve Connection After Being Subjected to High Temperature. *Ind. Constr.* **2022**, *52*, 106–112,71.
25. Chen, H.; Zhou, J.; Wang, B. Experimental study on mechanical properties of sleeve grouting material after fire. *J. Saf. Sci. Technol.* **2022**, *18*, 145–151.
26. Zhang, W.; He, C.; Zhang, J.; Ding, X.; Wang, Z.; Yi, W. Experimental study and bond slip analysis on mechanical properties of half grout sleeve splicing of rebars after high temperature. *J. Hunan Univ.* **2019**, *46*, 33–41.
27. Lin, F.; Wu, X. Mechanical performance and stress-strain relationships for grouted splices under tensile and cyclic loadings. *Int. J. Concr. Struct. Mater.* **2016**, *10*, 435–450. [[CrossRef](#)]
28. Yan, Q.; Chen, T.; Xie, Z. Seismic experimental study on a precast concrete beam-column connection with grout sleeves. *Eng. Struct.* **2018**, *155*, 330–344. [[CrossRef](#)]
29. Li, Y.; Zhang, L.; Zhang, Q.; He, X.; Wang, J.; Su, Y. Anchorage behavior of grouting sleeves under uniaxial and cyclic loading-A comparative study of the internal structure of sleeves. *J. Build. Eng.* **2022**, *49*, 104057. [[CrossRef](#)]
30. Zhao, X.L.; Grundy, P.; Lee, Y.T. Grout sleeve connections under large deformation cyclic loading. In Proceedings of the ISOPE International Ocean and Polar Engineering Conference, Kitakyushu, Japan, 26–31 May 2002.
31. Zheng, G.; Kuang, Z.; Xiao, J.; Pan, Z. Mechanical performance for defective and repaired grouted sleeve connections under uniaxial and cyclic loadings. *Constr. Build. Mater.* **2020**, *233*, 117233. [[CrossRef](#)]
32. Liu, Q.; Li, J.; Li, M.; Wu, X.; Li, Y.; Zhang, L. Bond performance prediction model of defective grout in post-fire sleeve connections under cyclic loading. *Constr. Build. Mater.* **2023**, *400*, 132442. [[CrossRef](#)]
33. Liu, Q.; Lin, Y.; Li, J.; Yang, C.; Chen, J.; Zhang, M.; Liu, B. Bond strength prediction model of defective grout materials in half-grouted sleeve connections under uniaxial and cyclic loadings. *Constr. Build. Mater.* **2022**, *352*, 128981. [[CrossRef](#)]

34. *JG/T 398-2019*; The Grouting Sleeve for Rebars Splicing. Ministry of Housing and Urban-Rural Development of China: Beijing, China, 2019.
35. *GB/T 17671-2021*; Test Method of Cement Mortar Strength (ISO Method). State Administration for Market Regulation of the People's Republic of China: Beijing, China, 2021.
36. Liu, Y.J.; Li, C.; Zhou, W.J. Numerical analysis on tensile properties of grout-filled splice sleeve rebars under ISO 834 standard fire. In *E3S Web of Conferences*; EDP Sciences: Les Ulis, France, 2018; Volume 38, p. 03036.
37. *GB/T 9978.2-2019*; Fire Resistance Tests—Elements of Building Construction—Part 2: Guidance on Measuring Uniformity of Furnace Exposure on Test Samples. State Administration for Market Regulation of the People's Republic of China & Standardization Administration of the People's Republic of China: Beijing, China, 2019.
38. *GB 50010-2010*; Code for Design of Concrete Structures. Ministry of Housing and Urban-Rural Development of China: Beijing, China, 2010.

Disclaimer/Publisher's Note: The statements, opinions and data contained in all publications are solely those of the individual author(s) and contributor(s) and not of MDPI and/or the editor(s). MDPI and/or the editor(s) disclaim responsibility for any injury to people or property resulting from any ideas, methods, instructions or products referred to in the content.